

PhysMamba: State Space Duality Model for Remote Physiological Measurement

Zhixin Yan¹, Yan Zhong², Hongbin Xu³, Wenjun Zhang², Lin Shu¹, Hongbin Xu³, Wenxiong Kang³

¹School of Future Technology, South China University of Technology, Guangzhou, China

²School of Electronic and Information Engineering, South China University of Technology, Guangzhou, China

³School of Automation Science and Engineering, South China University of Technology, Guangzhou, China

Abstract

Remote Photoplethysmography (rPPG) is a non-contact technique for extracting physiological signals from facial videos, used in applications like emotion monitoring, medical assistance, and anti-face spoofing. Unlike controlled laboratory settings, real-world environments often contain motion artifacts and noise, affecting the performance of existing rPPG methods. To address this, we propose PhysMamba, a dual-Pathway time-frequency interaction model via State Space Duality. This method allows the network to learn richer, more representative features, enhancing robustness in noisy conditions. To facilitate information exchange and feature complementation between the two pathways, we design an improved algorithm: Cross-Attention State Space Duality (CASSD). We conduct comparative experiments on the PURE, UBFC-rPPG, and MMPD datasets. Experimental results show that PhysMamba achieves state-of-the-art performance, particularly in complex environments, demonstrating its potential in practical remote physiological signal measurement applications.

Introduction

Photoplethysmography (PPG) is a common physiological parameter used to estimate heart rate, heart rate variability, respiratory rate, and other indicators, aiding in the analysis of physiological and psychological states. These analyses are widely applied in sleep monitoring, medical assistance, and fatigue monitoring. Traditionally, physiological parameter acquisition required contact-based devices like ECG monitors and PPG sensors, limiting practical applications. To address this, non-contact physiological signal estimation methods based on remote photoplethysmography (rPPG) have emerged (Chen et al. 2018; Liu, Patel, and McDuff 2021; Yu, Li, and Zhao 2021; Choi, Kang, and Kim 2024; Du et al. 2023). This technology uses cameras to capture optical signals from blood flow changes in the skin, estimating physiological parameters through advanced algorithms, thus overcoming the limitations of contact-based devices and expanding their application.

Early rPPG heart rate estimation research mainly relied on traditional signal processing techniques to capture periodic pulse wave signals (Li et al. 2014; Magdalena Nowara et al.

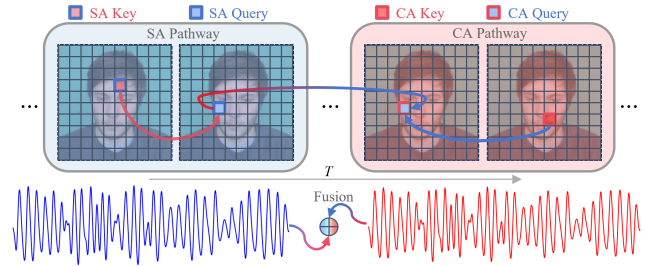


Figure 1: Information Interaction in the Dual-Pathway Model. The Self-Attention (SA) pathway computes attention using SA Key and SA Query. The Cross-Attention (CA) pathway uses the CASSD module to replace the original CA Query with the SA Query. The CA Key then computes cross-attention with the SA Query, enabling information exchange between the pathways.

2018; Poh, McDuff, and Picard 2010a; Tulyakov et al. 2016; Wang et al. 2016; Hsu, Ambikapathi, and Chen 2017; Niu et al. 2018, 2019a; Qiu et al. 2018). These methods initially identified periodic changes in rPPG but struggled with weak signals due to artifacts and noise, requiring complex preprocessing and lacking effective contextual integration. With the rapid development of deep learning, end-to-end methods using CNNs and Transformers (Han et al. 2022) have become main pathway. However, CNNs have limitations in handling long-range dependencies, while Transformers, despite capturing long-range dependencies, involve quadratic computational costs, limiting their efficiency and scalability (Xu et al. 2024).

Recently, the state space models (SSMs) proposed by Mamba (Gu and Dao 2023) has been applied to several Artificial Intelligence (AI) tasks (Ma et al. 2024; Ma, Li, and Wang 2024; Chen et al. 2024; Li et al. 2024; Yang, Xing, and Zhu 2024), including rPPG signal estimation (Zou et al. 2024), due to its linear time complexity and ability to capture long-term dependencies. However, the utilized Mamba-1 in (Zou et al. 2024) has limitations in parallel processing and generalization due to its dependency on previous states. To overcome these, Mamba-2 (Dao and Gu 2024) introduced the State Space Duality (SSD) framework, combining the linear time complexity of SSMs with the feature extraction capa-

bilities of attention mechanisms. The SSD algorithm optimizes computation using block decomposition and matrix multiplication, and integrates multi-head attention, enhancing adaptability and accuracy in identifying periodic rPPG features.

To enhance rPPG estimation in scenarios characterized by noise and motion artifacts, we propose PhysMamba, a remote physiological signal estimation model via State Space Duality. SSD was chosen for its computational efficiency and learning capability, combining SSMs’ long-term dependency capture with Transformers’ flexible attention. Recognizing that single-path networks struggle with complex scenarios, we design a dual-pathway network to learn richer feature representations, significantly improving robustness. The Cross-Attention Mechanism State Space Duality (CASSD) module was introduced to ensure effective information sharing and complementary attention between pathways, avoiding redundant information and enhancing performance. Ablation experiments demonstrated CASSD’s significant performance enhancement. PhysMamba supports efficient processing of diverse physiological signals, ensuring optimal learning and generalization under various conditions, validating its effectiveness and providing new directions for practical remote Physiological Measurement.

The main contributions are summarized as follows:

- We propose PhysMamba, an efficient rPPG estimation method via State Space Duality in a dual-pathway time-frequency interactive network. This is the first attempt handling rPPG estimation via SSD, creating technological breakthroughs.
- To enhance information exchange in dual-pathway model, we develop a simple state space fusion module using cross-attention for effective lateral information sharing, improving robustness and generalization.
- Extensive experiments on three public rPPG datasets of varying difficulty levels, including internal and cross-dataset testing, show that PhysMamba achieves state-of-the-art performance in rPPG heart rate estimation, demonstrating its superior robustness and generalization capabilities.

Related Work

rPPG Estimation

Early rPPG estimation methods used traditional signal processing techniques(Li et al. 2014; Magdalena Nowara et al. 2018; Poh, McDuff, and Picard 2010a; Tulyakov et al. 2016), such as extracting color channels from facial regions of interest (ROI), and signal decomposition methods like independent component analysis (ICA) and matrix completion. Techniques like chrominance subspace projection(De Haan and Jeanne 2013; Wang et al. 2016) and skin orthogonal space were also used. Despite their ability to extract rPPG signals, these methods had limitations, including reliance on prior knowledge and complex preprocessing. With the rise of deep learning, rPPG estimation methods evolved into non-end-to-end and end-to-end approaches. Non-end-to-end methods included predefined facial ROIs in

different color spaces to extract STmaps(Niu et al. 2018, 2019b) or their variants, and multi-scale STmaps(Lu, Han, and Zhou 2021; Niu et al. 2020), followed by cascaded CNNs(He et al. 2016) and RNNs(Cho et al. 2014) for feature extraction. However, these methods still required manual feature extraction and struggled with significant head movements. End-to-end methods, including CNN-based(Chen and McDuff 2018; Niu et al. 2019a, 2020) and Transformer-based approaches(Yu et al. 2022, 2023), addressed these issues but faced challenges in handling long-range dependencies and high computational complexity, affecting performance in complex scenarios like VIPL-HR(Niu et al. 2019a) and MMPD(Tang et al. 2023) datasets.

State Space Model

In order to enhance the capture of contextual information within lengthy sequences, SSMs have garnered significant interest(Gu et al. 2022). The Mamba SSM(Gu and Dao 2023) maintains linear time complexity while effectively capturing long-term dependencies, and has been successfully applied in various AI fields such as time series analysis(Ma et al. 2024), medical image segmentation(Ma, Li, and Wang 2024), and video understanding(Chen et al. 2024; Li et al. 2024; Yang, Xing, and Zhu 2024). Recently, Mamba has been used for rPPG estimation, achieving good results with low computational complexity. Bochao Zou and his team proposed RhythmMamba(Zou et al. 2024), an SSM-based method that robustly identifies quasi-periodic patterns in rPPG signals using a multi-phase learning framework and a frequency-domain feedforward mechanism. However, the utilized Mamba-1 in (Zou et al. 2024) had limitations in efficiency and generalization due to its dependency on previous states. Mamba-2(Dao and Gu 2024) introduced the State Space Duality framework, enhancing the combination of SSMs’ linear time complexity with attention mechanisms’ feature representation capabilities. This framework improves efficiency and generalization, offering new possibilities for complex physiological signal estimation tasks like rPPG.

Methodology

Overall Framework

PhysMamba is an end-to-end model that takes raw facial video data as input and directly produces the predicted rPPG signals. The overall framework is illustrated in Figure 2. PhysMamba features two pathways: the Self-Attention (SA) Pathway and the Cross-Attention (CA) Pathway. Each pathway includes a Frame Stem, Multi-temporal Cross Attention SSD, and a Frequency Domain Feed Forward (FDF) network. The outputs from both pathways are fused and then passed to the rPPG Predictor for final rPPG signal estimation.

The input video data $X \in \mathbb{R}^{3 \times T \times H \times W}$ is initially processed in the Frame Stem to produce $X_{stem} \in \mathbb{R}^{T/2 \times C}$. This stage involves processing X through convolutional layers, pooling layers, and Batch Normalization (BN) layers, integrating spatial information into the channel dimension for preliminary rPPG extraction. A masked self-attention

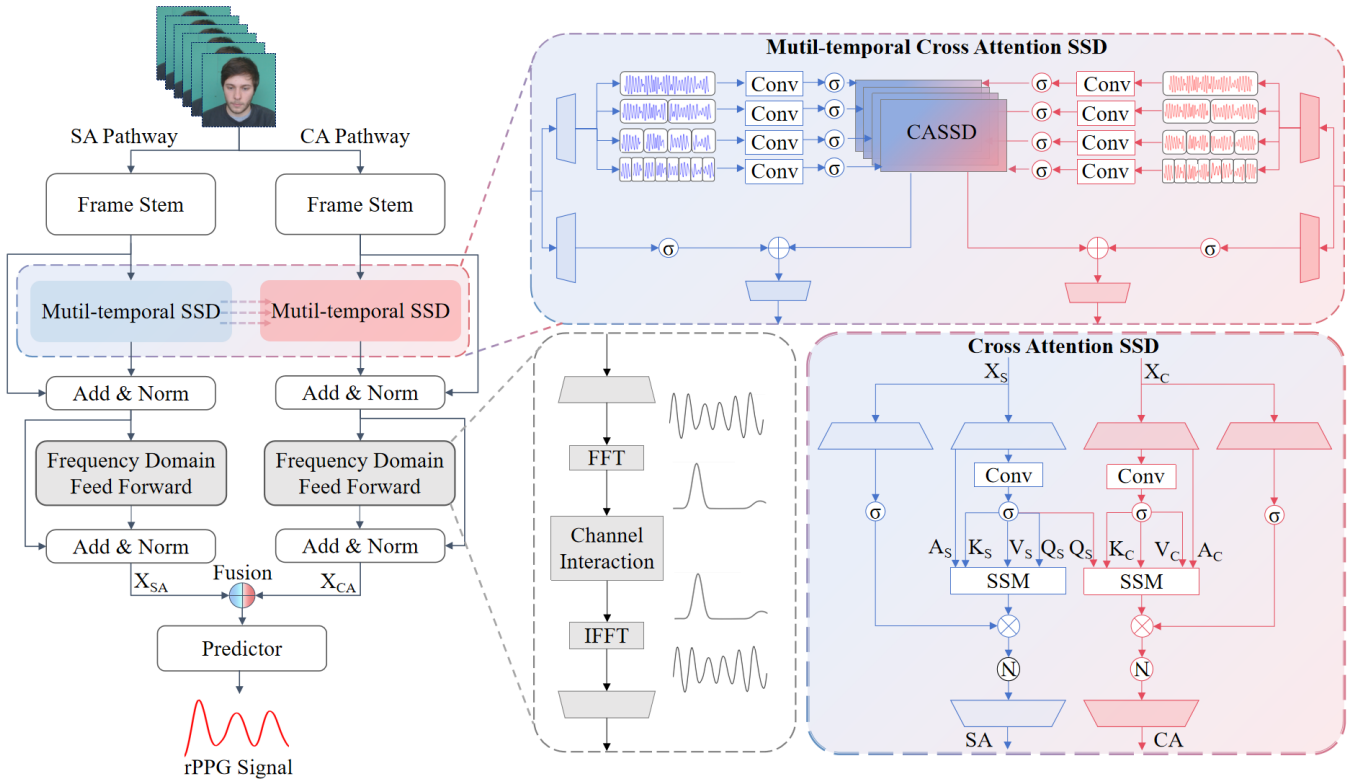


Figure 2: Overall framework diagram of the PhysMamba model. The model is divided into two pathways, namely the SA Pathway and the CA Pathway, and is generally composed of the Frame Stem, Multi-temporal Cross Attention SSD, Frequency Domain Feed-forward, and rPPG Predictor sections.

mechanism focuses on the facial area, enhancing feature representation, with the output denoted as X_{Stem} . The input X_{Stem} is directed into the Multi-temporal Cross-Attention SSD, which partitions tokens into sequences of different time spans, enabling effective feature extraction and information interchange via the dual pathways. Moreover, the Frequency Domain Feed Forward network amalgamates frequency domain details into the channels, thereby boosting the model’s capacity to discern the periodic attributes of the signal. Finally, the outputs from both pathways are concatenated and input into the rPPG Predictor, which outputs the predicted rPPG signals through a one-dimensional convolutional layer.

Frame Stem

Research (Zou et al. 2024) indicates that spatial information can interfere with the linear SSM model’s parsing of temporal information. Hence, the Frame Stem module is crafted to extract temporal features at the outset and fuse them with spatial data within the channels, mitigating interference during subsequent time-frequency interactions.

Firstly, differential frame processing is carried out: the video frames are processed to calculate the differences between consecutive frames, such as sequentially computing the differences between X_{t-2} , X_{t-1} , X , X_{t+1} , X_{t+2} , to capture subtle changes between frames. The Stem module

cascades a 2D-CNN with a 7×7 kernel size, a Batch Normalization (BN) layer, a ReLU activation function, and a Max Pooling layer. Both the original frames and the differential frames are processed through the Stem for preliminary feature extraction, yielding outputs X_{origin} and X_{diff} respectively. Afterward, X_{origin} and X_{diff} are combined, and the feature representation is further enhanced by passing through the Stem module again.

$$X_{Stem} = \text{Stem}(X_{origin}) + \text{Stem}(X_{origin} + X_{diff}). \quad (1)$$

After fusion, X_{Stem} undergoes further processing through a 5×5 convolution, followed by a self-attention mechanism designed to highlight key features in the facial area. This mechanism adaptively focuses on the most informative parts of the video. The self-attention mask can be represented as:

$$\text{Mask} = \frac{(H/8)(W/8) \cdot (\text{Conv}(X_{Stem}))}{2 \|\|\text{Conv}(X_{Stem})\|\|_1}. \quad (2)$$

Finally, the attention output $X_{attn} \in \mathbb{R}^{C \times T/2 \times H/8 \times W/8}$ is subjected to an average pooling operation along the spatial dimensions (i.e., height and width) to obtain the output $X_{stem} \in \mathbb{R}^{T/2 \times C}$.

Multi-temporal Cross Attention SSD

To precisely capture the contextual interactions and periodic changes within long sequence frames, and to meticulously

attend to the temporal cues between short sequence frames, we introduce a multi-temporal learning strategy. By utilizing sliding windows of four different lengths, we construct sequences composed of segments of varying durations (Figure 2), enabling the SSM block to be simultaneously influenced by the periodicity of long sequences and the trendiness of short sequences. After further processing through convolutional and activation layers, these sequences provide the SSM block with a more enriched and nuanced set of temporal features.

The State Space Model (SSM) is a mathematical framework that uses a set of linear equations to describe the evolution of a system’s state over time. The SSM is modeled through the following equations, which define how the state changes over time and how inputs are mapped to outputs:

$$\begin{aligned} h_t &= Ah_{t-1} + Bx_t, \\ y_t &= C^\top h_t, \end{aligned} \quad (3)$$

The SSM models the evolution of the state over time through the state transition matrix A , the input matrix B maps the input x to the state space, and the output matrix C maps the state space to the output space.

The attention mechanism allows the model to focus on important parts when processing sequence data. In Transformer models, attention is implemented by calculating the relationships between the queries (Q), keys (K), and values (V). The attention mechanism is typically defined by the following formula:

$$\text{Attention}(Q, K, V) = \text{softmax}\left(\frac{QK^\top}{\sqrt{d_k}}\right)V, \quad (4)$$

where d_k is the dimension of the keys.

In (Dao and Gu 2024), the State Space Duality framework combines State Space Models with an attention mechanism to enhance the model’s ability to process sequential data. SSD introduces a structured mask matrix L to control state transitions, replacing the traditional softmax operation, thereby achieving a function similar to the attention mechanism and enabling attention computation with linear time complexity. The formula is expressed as follows:

$$\text{SSD} = (L \circ QK^\top) \cdot V, \quad (5)$$

Map A , K , Q , and V in parallel at the start of each block. Use a data-dependent position mask matrix L to control information propagation over time, replacing heuristic position embeddings.

To further enhance the model’s learning ability and robustness, PhysMamba introduces a dual-pathway model. To avoid potential redundancy from independent pathways, we design the Cross-Attention State Space Duality (CASSD) algorithm, the schematic and details are shown in Figure 1 and Figure 2. This module facilitates information sharing and complementary advantages by sharing feature information between the two pathways. We designate one pathway as the Self-Attention (SA) Pathway and the other as the Cross-Attention (CA) Pathway. By passing the Q from the SA Pathway to the CA Pathway, an attention connection is established between the two pathways. This allows the CA

Pathway to learn not only through self-attention but also to refine its features with information from the other pathway, enabling mutual constraint and mutual promotion between the dual pathways. This design endows the model with more robust performance. The attention outputs for the two pathways are:

$$\text{SA} = (L_S \circ Q_S K_S^\top) \cdot V_S. \quad (6)$$

$$\text{CA} = (L_C \circ Q_S K_C^\top) \cdot V_C. \quad (7)$$

Frequency Domain Feed-forward

In rPPG heart rate estimation, frequency domain features are crucial for accurately identifying heart rate peaks. Our model uses a Frequency Domain Feed-forward (FDF) network to integrate these features effectively.

As shown in Figure 2, Multi-temporal Cross Attention SSD extracts time-domain signals, which are then transformed into the frequency domain using Fast Fourier Transform (FFT). The formula 8 represents the input time series $h(t)$ and the output frequency domain features $H(f)$:

$$\begin{aligned} H(f) &= \int_{-\infty}^{+\infty} h(t)e^{-j2\pi ft} dt \\ &= \int_{-\infty}^{+\infty} h(t) \cos(2\pi ft) dt + j \int_{-\infty}^{+\infty} h(t) \sin(2\pi ft) dt \\ &= H(f)_{\text{re}} + jH(f)_{\text{im}}. \end{aligned} \quad (8)$$

This conversion enables interaction between multi-channel signals, enhancing the model’s ability to recognize periodic characteristics. The inverse Fourier transform then converts the signals back to the time domain, retaining original temporal information enriched by frequency domain processing.

The model ultimately outputs features that combine time and frequency information, ensuring accurate and reliable heart rate estimation. This design allows the model to focus on heart rate signals, improving rPPG heart rate estimation’s accuracy and robustness.

rPPG Predictor

After the previous steps, the data from the two pathways is concatenated along the channel dimension:

$$X_{\text{fusion}} = \text{Concat}(X_{CA}, X_{SA}). \quad (9)$$

This step integrates the rich time-frequency features extracted from different processing stages by the two pathway models. The concatenated features are then processed through a one-dimensional convolutional layer and subsequently flattened into a long sequence, with the flattened sequence representing the predicted values of the rPPG signal.

Experiments

Dataset

To comprehensively evaluate PhysMamba’s performance, we selected three public rPPG datasets: two simpler

Method	UBFC				PURE				MMPD				
	MAE	RMSE	MAPE	r	MAE	RMSE	MAPE	r	MAE	RMSE	MAPE	r	SNR
GREEN	19.73	31.00	18.72	0.37	10.09	23.85	10.28	0.34	21.68	27.69	24.39	-0.01	-14.34
ICA	16.00	25.65	15.35	0.44	4.77	16.07	4.47	0.72	18.60	24.30	20.88	0.01	-13.84
CMROM	4.06	8.83	3.34	0.89	5.77	14.93	11.52	0.81	13.66	18.76	16.00	0.08	-11.74
LGI	15.80	28.55	14.70	0.36	4.61	15.38	4.96	0.77	17.08	23.32	18.98	0.04	-13.15
PBV	15.90	26.40	15.17	0.48	3.92	12.99	4.84	0.84	17.95	23.58	20.18	0.09	-13.88
POS	4.08	7.72	3.93	0.92	3.67	11.82	7.25	0.88	12.36	17.71	14.43	0.18	-11.53
OMIT	15.79	28.54	14.69	0.36	4.65	15.81	4.96	0.75	7.80	12.00	10.55	0.13	-8.68
DeepPhys	0.76	1.09	0.79	0.99	3.33	14.45	2.91	0.90	23.73	28.25	25.63	-0.06	-15.45
PhysNet	0.58	0.83	0.61	0.99	0.54	0.93	0.58	0.99	4.81	11.83	4.84	0.60	1.51
TS-CAN	0.81	1.10	0.84	0.99	0.40	0.73	0.44	0.99	8.97	16.58	9.43	0.44	-6.92
PhysFormer	0.63	0.98	0.65	0.99	0.25	0.37	0.34	0.99	13.64	19.39	14.42	0.15	-11.02
EfficientPhys	0.72	1.01	0.75	0.99	5.10	16.61	4.19	0.87	12.79	21.12	13.48	0.24	-9.23
RhythmMamba	0.54	0.79	0.54	0.99	0.29	0.39	0.36	0.99	3.16	7.27	3.37	0.84	4.74
PhysMamba(Ours)	0.45	0.76	0.45	0.99	0.24	0.36	0.31	0.99	2.84	6.41	3.04	0.88	5.20

Table 1: Intra-dataset results for UBFC, PURE and MMPD datasets.

ones, UBFC-rPPG(?) and PURE(?), and a complex one, MMPD(Tang et al. 2023), which features high levels of noise and motion artifacts.

UBFC-rPPG: This dataset includes facial videos from 42 subjects, providing PPG waveforms and corresponding heart rate labels. Subjects participated in a mathematical game to induce natural heart rate variability during data collection.

PURE: This dataset comprises ten subjects (eight males and two females) and records their pulse measurements during six controlled head movements: stillness, speaking, slow horizontal rotation, fast horizontal rotation, small vertical rotation, and medium vertical rotation.

MMPD: This challenging dataset involves 33 subjects with four different skin tones, collecting 11 hours of mobile phone videos. It considers four lighting levels, three light sources, and four movement difficulty levels. MMPD provides multiple labels, including skin tone, gender, eyeglass wearing, hair coverage rate, and makeup, to assess model generalization and robustness. Specifically, we used the mini-MMPD version due to experimental design and computational resource limitations.

Extensive experiments confirmed PhysMamba’s effectiveness across various difficulty levels and scenarios, highlighting its excellent performance with complex environmental variables and physiological changes. These results demonstrate its reliability and accuracy in heart rate estimation. We evaluate methods using metrics like Mean Absolute Error (MAE), Root Mean Squared Error (RMSE), Mean Absolute Percentage Error (MAPE), and Pearson correlation coefficient (r). For the noisy MMPD dataset, we increase the Signal-to-Noise Ratio (SNR) for evaluation. These rigorous settings ensure a comprehensive assessment of PhysMamba’s reliability and effectiveness in practical applications.

Experimental Details

Our entire experiment was conducted using the open-source toolbox, rppg-toolbox, based on PyTorch. We followed the protocol(Zou et al. 2024), cropping and scaling the facial area in the first frame to 128×128, fixing this area in subsequent frames. A second-order Butterworth filter (cutoff frequencies: 0.75 and 2.5 Hz) was used to filter the predicted PPG waveform. The Welch algorithm then calculated the power spectral density for heart rate estimation. The learning rate was set to 3e-4, with a batch size of 16, over 30 epochs. The SSD has a model dimension and state space size all set to 64, head dimension set to 16. Our experiments are conducted on the NVIDIA RTX 4090.

Loss The loss function combines time-domain and frequency-domain losses. The time-domain loss L_{Time} is the negative Pearson correlation coefficient between the predicted rPPG signal and the true BVP label. The frequency-domain loss L_{Freq} is the cross-entropy loss between the frequency-domain transformation of the predicted rPPG signal and the true BVP label. To stabilize model training and prevent overfitting, the total loss function is defined as: $\mathcal{L}_{overall} = L_{Time} + L_{Freq}$.

Experimental Evaluation

To fully verify PhysMamba’s effectiveness and superiority in rPPG heart rate estimation, we have designed a detailed evaluation process, including both intra-dataset and cross-dataset assessments. We compared PhysMamba with Unsupervised methods including GREEN(Verkruyse, Svaasand, and Nelson 2008), ICA(Poh, McDuff, and Picard 2010b), CHROM(De Haan and Jeanne 2013), LGI(Pilz et al. 2018), PBV(De Haan and Van Leest 2014), and POS(Wang et al. 2016), OMIT(?), as well as state-of-the-art deep learning methods including DeepPhys(Chen and McDuff 2018), PhysNet(Yu, Li, and Zhao 2019), TS-CAN(Liu et al. 2020), PhysFormer(Yu et al. 2022),EfficientPhys(Liu et al. 2023),

Method	Train set	Test Set			
		PURE			
		MAE	RMSE	MAPE	r
DeepPhys		15.86	25.72	20.76	-0.01
PhysNet		10.96	20.24	18.34	0.54
TS-CAN		7.24	16.80	9.76	0.68
PhysFormer	MMPD	17.60	24.75	26.93	0.00
EfficientPhys		5.68	16.59	6.26	0.70
RhythmMamba		6.07	14.43	9.66	0.78
PhysMamba(Ours)		5.32	12.98	9.56	0.84

Table 2: Results trained on MMPD and tested on PURE

Method	Train set	Test Set			
		MMPD			
		MAE	RMSE	MAPE	r
DeepPhys		16.92	24.61	18.54	0.05
PhysNet		13.94	21.61	15.15	0.20
TS-CAN		13.94	21.61	15.15	0.20
PhysFormer	PURE	14.57	20.71	16.73	0.15
EfficientPhys		14.03	21.62	15.32	0.17
RhythmMamba		10.45	16.49	12.20	0.37
PhysMamba(Ours)		9.87	15.47	11.76	0.40

Table 3: Results trained on PURE and tested on MMPD

and RhythmMamba(Zou et al. 2024). The best results are highlighted in bold.

Intra-Dataset Testing: The intra-dataset evaluation phase tests PhysMamba’s performance on various datasets. UBFC-rPPG dataset: Data from the first 30 subjects were used for training, and data from the last 12 subjects for testing. PURE dataset: Data were divided with 60% for training and 40% for testing. MMPD dataset: Following (Zou et al. 2024), we divided the dataset into training, validation, and test sets in a 7:1:2 ratio.

Table 1 shows the performance on UBFC, PURE, and MMPD. PhysMamba matches state-of-the-art methods. With simpler datasets like PURE and UBFC-rPPG nearing performance limits, the MMPD dataset validates PhysMamba’s superiority due to its complex characteristics. Testing PhysMamba on the MMPD dataset, with its diverse conditions and characteristics, thoroughly examines the model’s adaptability to complex scenarios. PhysMamba achieved an MAE of 2.84, an RMSE of 6.41, an MAPE of 3.04, and a correlation coefficient of 0.88, on the MMPD dataset, the best among all compared methods. Since MMPD belongs to a dataset with high noise levels, we introduced the signal-to-noise ratio for further evaluation. It can be observed that PhysMamba has the highest SNR, indicating effective learning of the rPPG signal. This result verifies PhysMamba’s high accuracy and reliability in heart rate estimation, even in complex scenarios, demonstrating its strong robustness.

Cross-Dataset Testing In order to further validate the robustness and generalization of PhysMamba in noisy condi-

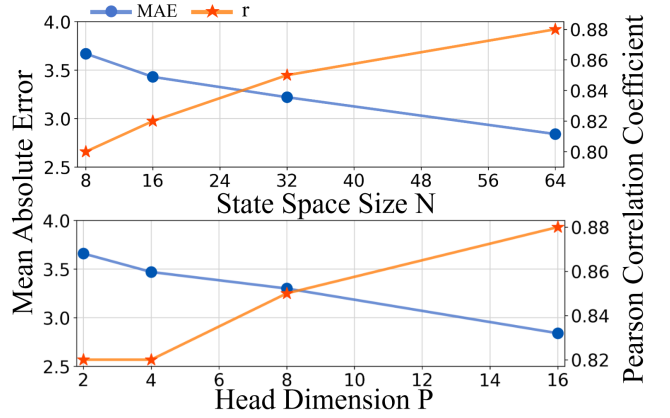


Figure 3: Impact of state space size and head dimension. Keeping P at 16, the value of N is increased. Keeping N at 64, the value of P is increased.

tions, we designed cross-dataset experiments. We selected the MMPD dataset, which contains a large amount of noise and motion artifacts, and the PURE dataset, which includes head movements. We trained on one dataset and tested on the other, with the training dataset split into training and validation sets in an 8:2 ratio. This is a highly challenging task that tests the model’s ability to learn effective features under noise or head motion conditions, as well as its inference generalization across noisy datasets.

As shown in the table2 and the table3, PhysMamba performs optimally under all conditions, indicating its ability to learn effective and generalizable features even in the presence of noise and significant motion artifacts. Furthermore, in the inference across noisy datasets, PhysMamba can still effectively predict rPPG signals, demonstrating its superior robustness and generalization capabilities.

Ablation Study

Impact of state space size and head dimension The state space size N in state space duality determines information storage, while the head dimension P in multi-head attention determines the number of features processed by each head. Both parameters affect the model’s learning ability. To find optimal values, we fixed the model dimension at 64 and examined MAE and r trends as state space size and head count increased. Figure 3 shows that as these increase, MAE decreases and r increases, indicating improved feature learning under noisy conditions. In the future, we will explore increasing the state space size, head dimension, and model dimension to enhance the model’s expressiveness and boost its performance in real-world applications.

Ablation of Key Module To assess the effectiveness of each core module, we performed ablation studies on the MMPD dataset, focusing on Multi-temporal, FDF, Dual-pathway, SSD, and Cross-Attention. Results are in Table 4. Module Description: Without Multi-temporal, input is a time block of length $T/2$. Without FDF, excludes the frequency domain feedforward network. Without Dual-pathway, only a single pathway is used. Without SSD, replaced by SSM only.

Multi-temporal	FDF	Dual-pathway	SSD	Cross-Attention	MAE	RMSE	MAPE	r	SNR
✓	✓				4.40	8.81	4.66	0.76	3.36
✓	✓		✓		3.46	7.21	3.69	0.84	3.94
✓	✓	✓			3.13	6.55	3.31	0.87	4.63
✓	✓	✓	✓		3.72	8.06	3.95	0.80	4.15
✓	✓	✓	✓	✓	3.53	7.46	3.83	0.82	1.50
	✓	✓	✓	✓	3.49	7.35	3.69	0.83	4.17
✓	✓	✓	✓	✓	2.84	6.41	3.04	0.88	5.20

Table 4: Ablation Study of the Key Module

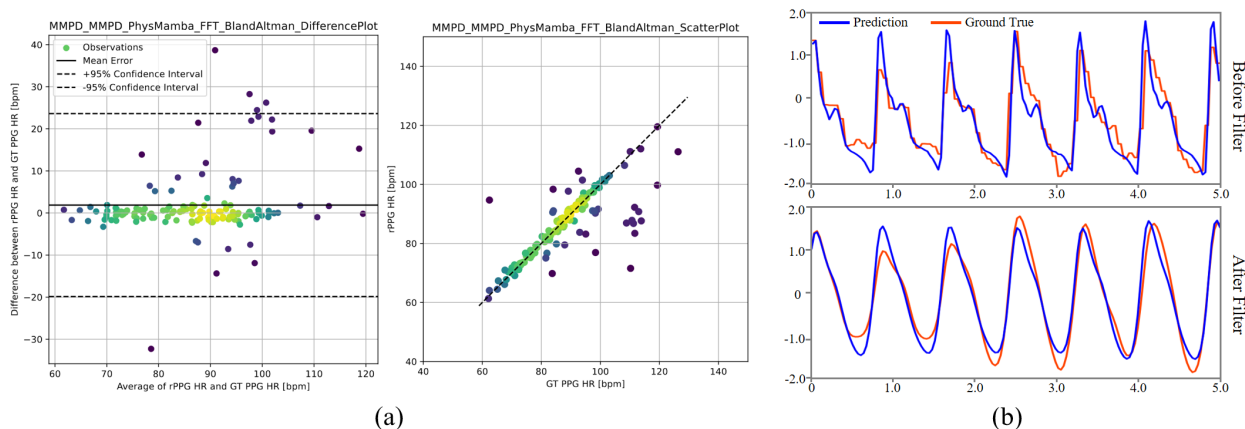


Figure 4: Visualization of the results from the MMPD dataset. (a) the Bland-Altman plot. (b) the waveform of a sample before and after filtering.

Without Cross-Attention, branch models do not exchange attention.

- **Impact of Time-Frequency Interaction.** Observing the fifth line, the frequency domain feedforward network effectively integrates frequency features into the channels, enabling time-frequency interaction and improving the model’s capacity to detect the main peak heart rate.
- **Impact of Multi-Temporal Inputs.** It is apparent from the sixth line that the multi-temporal long-short signals enable the SSM to capture both the temporal context of long sequences and the temporal trends of short sequences.
- **Impact of Information Interaction in dual SSD.** SSD enhances performance by combining SSM modeling with flexible Attention focus. Moving from one to two pathways with SSM improves performance, highlighting the need for stronger learning in complex scenarios. SSD with two pathways slightly decreases performance due to redundancy. However, adding the CASSD module significantly boosts performance, improving information sharing and enhancing robustness and generalization.

Visualization

In Figure 4(a), we present the Bland-Altman plot for the MMPD dataset, showing a strong correlation between predicted and actual values. Figure 4(b) illustrates pre- and

post-filtering rPPG and BVP waveforms of a sample, the consistent peaks and troughs validate the model’s sequential prediction capability. This indicates that even in complex environments, PhysMamba maintains high accuracy, highlighting its robustness.

Conclusion

To improve rPPG signal capture in complex environments with noise and motion artifacts, we introduce PhysMamba, a dual-pathway time-frequency interactive model based on State Space Duality. PhysMamba uses the State Space Duality algorithm, integrating state-space equations with attention mechanisms to capture long-term dependencies and focus flexibly on sequence parts. Its dual-pathway network structure enhances robustness by learning diverse rPPG features. We develop a simple state space fusion module using cross-attention to facilitate effective information sharing between pathways, preventing redundancy and achieving complementary feature advantages. We validated PhysMamba on simpler datasets (UBFC-rPPG, PURE) and a complex one (MMPD) through intra- and cross-dataset experiments. Results demonstrate PhysMamba’s superior performance, especially in noisy conditions, highlighting its potential for efficient remote physiological measurement in real-world scenarios.

References

- Chen, G.; Huang, Y.; Xu, J.; Pei, B.; Chen, Z.; Li, Z.; Wang, J.; Li, K.; Lu, T.; and Wang, L. 2024. Video mamba suite: State space model as a versatile alternative for video understanding. *arXiv preprint arXiv:2403.09626*.
- Chen, W.; and McDuff, D. 2018. Deepphys: Video-based physiological measurement using convolutional attention networks. In *Proceedings of the european conference on computer vision (ECCV)*, 349–365.
- Chen, X.; Cheng, J.; Song, R.; Liu, Y.; Ward, R.; and Wang, Z. J. 2018. Video-based heart rate measurement: Recent advances and future prospects. *IEEE Transactions on Instrumentation and Measurement*, 68(10): 3600–3615.
- Cho, K.; Van Merriënboer, B.; Bahdanau, D.; and Bengio, Y. 2014. On the properties of neural machine translation: Encoder-decoder approaches. *arXiv preprint arXiv:1409.1259*.
- Choi, J.-H.; Kang, K.-B.; and Kim, K.-T. 2024. Fusion-Vital: Video-RF Fusion Transformer for Advanced Remote Physiological Measurement. In *Proceedings of the AAAI Conference on Artificial Intelligence*, volume 38, 1344–1352.
- Comas, J.; Ruiz, A.; and Sukno, F. 2022. Efficient remote photoplethysmography with temporal derivative modules and time-shift invariant loss. In *Proceedings of the IEEE/CVF conference on computer vision and pattern recognition*, 2182–2191.
- Dao, T.; and Gu, A. 2024. Transformers are SSMS: Generalized models and efficient algorithms through structured state space duality. *arXiv preprint arXiv:2405.21060*.
- De Haan, G.; and Jeanne, V. 2013. Robust pulse rate from chrominance-based rPPG. *IEEE transactions on biomedical engineering*, 60(10): 2878–2886.
- De Haan, G.; and Van Leest, A. 2014. Improved motion robustness of remote-PPG by using the blood volume pulse signature. *Physiological measurement*, 35(9): 1913.
- Du, J.; Liu, S.-Q.; Zhang, B.; and Yuen, P. C. 2023. Dual-bridging with adversarial noise generation for domain adaptive rppg estimation. In *Proceedings of the IEEE/CVF Conference on Computer Vision and Pattern Recognition*, 10355–10364.
- Gu, A.; and Dao, T. 2023. Mamba: Linear-time sequence modeling with selective state spaces. *arXiv preprint arXiv:2312.00752*.
- Gu, A.; Johnson, I.; Timalina, A.; Rudra, A.; and Ré, C. 2022. How to train your hippo: State space models with generalized orthogonal basis projections. *arXiv preprint arXiv:2206.12037*.
- Gupta, A. K.; Kumar, R.; Birla, L.; and Gupta, P. 2023. Radiant: Better rppg estimation using signal embeddings and transformer. In *Proceedings of the IEEE/CVF winter conference on applications of computer vision*, 4976–4986.
- Han, K.; Wang, Y.; Chen, H.; Chen, X.; Guo, J.; Liu, Z.; Tang, Y.; Xiao, A.; Xu, C.; Xu, Y.; et al. 2022. A survey on vision transformer. *IEEE transactions on pattern analysis and machine intelligence*, 45(1): 87–110.
- He, K.; Zhang, X.; Ren, S.; and Sun, J. 2016. Deep residual learning for image recognition. In *Proceedings of the IEEE conference on computer vision and pattern recognition*, 770–778.
- Hsu, G.-S.; Ambikapathi, A.; and Chen, M.-S. 2017. Deep learning with time-frequency representation for pulse estimation from facial videos. In *2017 IEEE international joint conference on biometrics (IJCB)*, 383–389. IEEE.
- Lee, E.; Chen, E.; and Lee, C.-Y. 2020. Meta-rppg: Remote heart rate estimation using a transductive meta-learner. In *Computer Vision—ECCV 2020: 16th European Conference, Glasgow, UK, August 23–28, 2020, Proceedings, Part XXVII 16*, 392–409. Springer.
- Lee, J. S.; Hwang, G.; Ryu, M.; and Lee, S. J. 2023. Lstc-rppg: Long short-term convolutional network for remote photoplethysmography. In *Proceedings of the IEEE/CVF Conference on Computer Vision and Pattern Recognition*, 6015–6023.
- Li, J.; Yu, Z.; and Shi, J. 2023. Learning motion-robust remote photoplethysmography through arbitrary resolution videos. In *Proceedings of the AAAI Conference on Artificial Intelligence*, volume 37, 1334–1342.
- Li, K.; Li, X.; Wang, Y.; He, Y.; Wang, Y.; Wang, L.; and Qiao, Y. 2024. Videomamba: State space model for efficient video understanding. *arXiv preprint arXiv:2403.06977*.
- Li, X.; Chen, J.; Zhao, G.; and Pietikainen, M. 2014. Remote heart rate measurement from face videos under realistic situations. In *Proceedings of the IEEE conference on computer vision and pattern recognition*, 4264–4271.
- Liu, X.; Fromm, J.; Patel, S.; and McDuff, D. 2020. Multi-task temporal shift attention networks for on-device contactless vitals measurement. *Advances in Neural Information Processing Systems*, 33: 19400–19411.
- Liu, X.; Hill, B.; Jiang, Z.; Patel, S.; and McDuff, D. 2023. Efficientphys: Enabling simple, fast and accurate camera-based cardiac measurement. In *Proceedings of the IEEE/CVF winter conference on applications of computer vision*, 5008–5017.
- Liu, X.; Patel, S.; and McDuff, D. 2021. RGB Camera-based Physiological Sensing: Challenges and Future Directions. *arXiv preprint arXiv:2110.13362*.

- Lokendra, B.; and Puneet, G. 2022. AND-rPPG: A novel denoising-rPPG network for improving remote heart rate estimation. *Computers in biology and medicine*, 141: 105146.
- Lu, H.; Han, H.; and Zhou, S. K. 2021. Dual-gan: Joint bvp and noise modeling for remote physiological measurement. In *Proceedings of the IEEE/CVF conference on computer vision and pattern recognition*, 12404–12413.
- Ma, J.; Li, F.; and Wang, B. 2024. U-mamba: Enhancing long-range dependency for biomedical image segmentation. *arXiv preprint arXiv:2401.04722*.
- Ma, S.; Kang, Y.; Bai, P.; and Zhao, Y.-B. 2024. FMamba: Mamba based on Fast-attention for Multivariate Time-series Forecasting. *arXiv preprint arXiv:2407.14814*.
- Magdalena Nowara, E.; Marks, T. K.; Mansour, H.; and Veeraraghavan, A. 2018. SparsePPG: Towards driver monitoring using camera-based vital signs estimation in near-infrared. In *Proceedings of the IEEE conference on computer vision and pattern recognition workshops*, 1272–1281.
- Niu, X.; Han, H.; Shan, S.; and Chen, X. 2018. Synrhythm: Learning a deep heart rate estimator from general to specific. In *2018 24th international conference on pattern recognition (ICPR)*, 3580–3585. IEEE.
- Niu, X.; Shan, S.; Han, H.; and Chen, X. 2019a. Rhythmnet: End-to-end heart rate estimation from face via spatial-temporal representation. *IEEE Transactions on Image Processing*, 29: 2409–2423.
- Niu, X.; Yu, Z.; Han, H.; Li, X.; Shan, S.; and Zhao, G. 2020. Video-based remote physiological measurement via cross-verified feature disentangling. In *Computer Vision—ECCV 2020: 16th European Conference, Glasgow, UK, August 23–28, 2020, Proceedings, Part II 16*, 295–310. Springer.
- Niu, X.; Zhao, X.; Han, H.; Das, A.; Dantcheva, A.; Shan, S.; and Chen, X. 2019b. Robust remote heart rate estimation from face utilizing spatial-temporal attention. In *2019 14th IEEE international conference on automatic face & gesture recognition (FG 2019)*, 1–8. IEEE.
- Pilz, C. S.; Zaunseder, S.; Krajewski, J.; and Blazek, V. 2018. Local group invariance for heart rate estimation from face videos in the wild. In *Proceedings of the IEEE conference on computer vision and pattern recognition workshops*, 1254–1262.
- Poh, M.-Z.; McDuff, D. J.; and Picard, R. W. 2010a. Advancements in noncontact, multiparameter physiological measurements using a webcam. *IEEE transactions on biomedical engineering*, 58(1): 7–11.
- Poh, M.-Z.; McDuff, D. J.; and Picard, R. W. 2010b. Non-contact, automated cardiac pulse measurements using video imaging and blind source separation. *Optics express*, 18(10): 10762–10774.
- Qiu, Y.; Liu, Y.; Arteaga-Falconi, J.; Dong, H.; and El Saddik, A. 2018. EVM-CNN: Real-time contactless heart rate estimation from facial video. *IEEE transactions on multimedia*, 21(7): 1778–1787.
- Song, R.; Chen, H.; Cheng, J.; Li, C.; Liu, Y.; and Chen, X. 2021. PulseGAN: Learning to generate realistic pulse waveforms in remote photoplethysmography. *IEEE Journal of Biomedical and Health Informatics*, 25(5): 1373–1384.
- Špetlík, R.; Franc, V.; and Matas, J. 2018. Visual heart rate estimation with convolutional neural network. In *Proceedings of the british machine vision conference, Newcastle, UK*, 3–6.
- Tang, J.; Chen, K.; Wang, Y.; Shi, Y.; Patel, S.; McDuff, D.; and Liu, X. 2023. Mmpd: multi-domain mobile video physiology dataset. In *2023 45th Annual International Conference of the IEEE Engineering in Medicine & Biology Society (EMBC)*, 1–5. IEEE.
- Tsou, Y.-Y.; Lee, Y.-A.; Hsu, C.-T.; and Chang, S.-H. 2020. Siamese-rPPG network: Remote photoplethysmography signal estimation from face videos. In *Proceedings of the 35th annual ACM symposium on applied computing*, 2066–2073.
- Tulyakov, S.; Alameda-Pineda, X.; Ricci, E.; Yin, L.; Cohn, J. F.; and Sebe, N. 2016. Self-adaptive matrix completion for heart rate estimation from face videos under realistic conditions. In *Proceedings of the IEEE conference on computer vision and pattern recognition*, 2396–2404.
- Verkruysse, W.; Svaasand, L. O.; and Nelson, J. S. 2008. Remote plethysmographic imaging using ambient light. *Optics express*, 16(26): 21434–21445.
- Wang, W.; Den Brinker, A. C.; Stuijk, S.; and De Haan, G. 2016. Algorithmic principles of remote PPG. *IEEE Transactions on Biomedical Engineering*, 64(7): 1479–1491.
- Xu, R.; Yang, S.; Wang, Y.; Du, B.; and Chen, H. 2024. A survey on vision mamba: Models, applications and challenges. *arXiv preprint arXiv:2404.18861*.
- Yang, Y.; Xing, Z.; and Zhu, L. 2024. Vivim: a video vision mamba for medical video object segmentation. *arXiv preprint arXiv:2401.14168*.
- Yu, Z.; Li, X.; Niu, X.; Shi, J.; and Zhao, G. 2020. Autohr: A strong end-to-end baseline for remote heart rate measurement with neural searching. *IEEE Signal Processing Letters*, 27: 1245–1249.
- Yu, Z.; Li, X.; and Zhao, G. 2019. Remote photoplethysmograph signal measurement from facial videos using spatio-temporal networks. *arXiv preprint arXiv:1905.02419*.
- Yu, Z.; Li, X.; and Zhao, G. 2021. Facial-video-based physiological signal measurement: Recent advances and affective applications. *IEEE Signal Processing Magazine*, 38(6): 50–58.

Yu, Z.; Shen, Y.; Shi, J.; Zhao, H.; Cui, Y.; Zhang, J.; Torr, P.; and Zhao, G. 2023. Physformer++: Facial video-based physiological measurement with slowfast temporal difference transformer. *International Journal of Computer Vision*, 131(6): 1307–1330.

Yu, Z.; Shen, Y.; Shi, J.; Zhao, H.; Torr, P. H.; and Zhao, G. 2022. Physformer: Facial video-based physiological measurement with temporal difference transformer. In *Proceedings of the IEEE/CVF conference on computer vision and pattern recognition*, 4186–4196.

Zhang, X.; Xia, Z.; Liu, L.; and Feng, X. 2023. Demodulation based transformer for rPPG generation and heart rate estimation. *IEEE Signal Processing Letters*.

Zou, B.; Guo, Z.; Hu, X.; and Ma, H. 2024. Rhythm-mamba: Fast remote physiological measurement with arbitrary length videos. *arXiv preprint arXiv:2404.06483*.